ACTA TECHNICA CORVINIENSIS
– Bulletin of Engineering
Tome X [2017]
Fascicule 4 [October – December]
ISSN: 2067 – 3809

[1, 2.]Fatai O. ARAMIDE, [1.]Idris B. AKINTUNDE, [2.]Patricia A. POPOOLA

EFFECTS OF TITANIA AND SINTERING TEMPERATURE ON THE PHASE DEVELOPMENT AND PROPERTIES OF SINTERED MULLITE-CARBON COMPOSITE SYNTHESIZED FROM OKPELLA KAOLIN

[1.]Department of Metallurgical and Materials Engineering, Federal University of Technology, P.M.B. 704, Akure, NIGERIA
[2.]Department of Chemical, Metallurgical and Materials Engineering, Tshwane University of Technology, Staatsartillerie Road, Pretoria West, SOUTH AFRICA

Abstract: The effects of the addition of titania and sintering temperatures on the phases developed, physical and mechanical properties of sintered ceramic composite produced from kaolin and spent graphite electrode was investigated. The kaolin and graphite of known mineralogical composition were thoroughly blended with 2 and 4 (vol.) % titania. From the homogeneous mixture of kaolin, graphite and titania, standard samples were prepared via uniaxial compaction. The test samples produced were subjected to firing (sintering) at 1300˚C, 1400˚C and 1500˚C. The sintered samples were characterized for the developed phases using x-ray diffractometry analysis, microstructural morphology using ultra-high resolution field emission scanning electron microscope (UHRFEGSEM) various physical and mechanical properties were determined. It was observed that microstructural morphology of the samples revealed the evolution of mullite, cristobalite and microcline. The mineralogical phase of the samples revealed the increments in the evolution of mullite and also the variation in other phase attained as the sintering temperature was raised from 1300˚C to 1500˚C for the sample having the same composition. It was concluded that the optimum mechanical property of the ceramic samples produced was achieved with sample that contain 4 (vol.) % titania and sintered at 1300˚C.
Keywords: titania; kaolin; carbon; sintering temperatures; phases developed; sintered ceramic composite

INTRODUCTION

Mullite-carbon composites find increasing applications as refractories in the context of recent developments in ceramic industry for high temperature applications [1]. These refractories exhibit in general a complex microstructure characterized by crystalline phases of different thermal expansion coefficients, physical and mechanical property. There is a current limited understanding about the effect of microstructural features, including residual thermal stresses, on the overall performance of mullite-carbon ceramic composite at high temperature.

Previous researches have exploit mullite-zirconia and the addition of various additives which have been widely used for high-temperature applications due to their superior physico-mechanical properties [2]. This composite will compete with the existing mullite-zirconia in its area of applications. Recently, many researchers have focused their investigations on how to improve the properties of ceramics for various applications; Rendtorff *et al*. (2008) [3] used two different processing routes: for the preparation of zirconia-mullite composites, which are reaction sintering of alumina and zircon and direct sintering of mullite-zirconia grains by slip casting and sintered at 1600˚C for 2 hours. Badiee *et al.* (2001) [4] studied the effect of CaO, MgO, TiO_2, and ZrO_2 on mullitization of the Iranian and alusite located in Hamedan mines. They found out that the first three of these additives encouraged mullite formation from and alusite. Ebadzadeh and Ghasemi, (2002) [5] prepared zirconia-mullite composites using α-alumina and aluminium nitrate and zircon powder with TiO_2 as additive. Aramide *et al.* (2014) [6] synthesized mullite-zirconia composites containing yttria as additive. Chandra *et al.* (2013) [7] prepared zirconia-toughened ceramics with a mullite matrix based on the quaternary system ZrO_2-Al_2O_3-SiO_2-TiO_2 in the temperature range 1450-1550˚C using zircon-alumina-titania mixtures. Aksel and Komicezny, (2001) [8] studied the influence of zircon on the mechanical properties and thermal shock behaviour of slip-cast alumina-mullite refractories.

Furthermore, Jiang *et al.* (2011) [9] demonstrated that the role of additives can be rationalized in terms of promotion of sintering process, formation of new phases and influence on lattice constant of aluminum titanate ceramics. Dong *et al.* (2008) [10], specified the effect of both single additives (MgO, SiO_2, Fe_2O_3 and ZrO_2) and compound additives on the mechanical and thermal properties of aluminum titanate ceramics, and finally pointed out that the compound additives of MgO and Fe_2O_3 have an excellent improvement on the stability of aluminum titanate. Aramide *et al.* (2016) [11] had synthesized mullite-carbon composite from the same materials without any additive. The objective of the present work is to improve the properties of the mullite-carbon ceramic composite through the use of titania.

MATERIALS AND METHODS

RAW MATERIALS

Clay sample used for this study (as mine Kaolin sample) was sourced from Okpella, Edo State southern part of Nigeria, Graphite and titania (TiO_2) were sourced from (Pascal Chemicals, Akure), this were used to maintain the granulometry of the mixture.

METHOD

» **Processing of raw materials (Graphite & Kaolin)**

The raw materials (Spent graphite electrode and kaolin) were crushed into a coarse particle size, of about 10 mm for graphite and less than 2mm for kaolin; the crushed samples were further reduced by grinding using Herzog rod mill. The powdered samples were sieved using 600µm sizes aperture according to ASTM standards in an electric sieve shaker. The undersize that passed through the 600µm sieve aperture were used in the samples making.

» **Phase and Mineralogical Composition of Raw Kaolin and Graphite**

The kaolin clay and graphite electrode samples were carefully prepared for these analyses by digesting in reagents as described by Nabil and Barbara, (2012) [12]. The mineralogical phases present in the samples were determined using X-ray diffractometry (XRD).

The samples were prepared for XRD analysis using a back loading preparation method. They were analyzed using a PANalytical X'Pert Pro powder diffractometer with X'Celerator detector and variable divergence- and receiving slits with Fe filtered Co-Kα radiation. The phases were identified using X'Pert Highscore plus software. The receiving slit was placed at 0.040°. The counting area was from 5 to 70° on a 2θ scale. The count time was 1.5s. The temperature-scanned XRD data were obtained using an Anton Paar HTK 16 heating chamber with Pt heating strip Graphical representations of the qualitative result follow below.

The relative phase amounts (weight %) was estimated using the Rietveld method (Autoquan Program) as reported by Young et al [13]. Amorphous phases, if present were not taken into consideration in the quantification. The phases are reported in Figures 1 and 2 and also in Table 1.

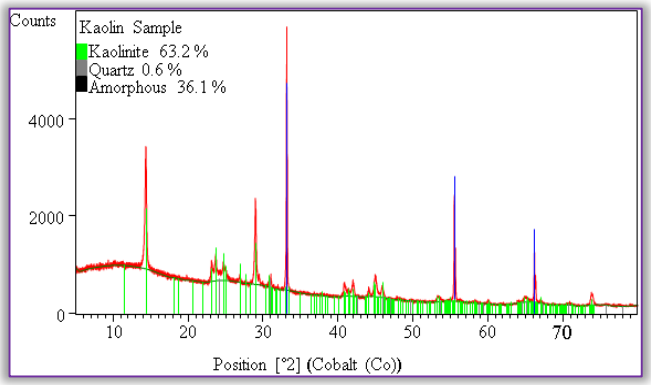

Figure 1. X-Ray Diffractometry Pattern (Phase Analysis) of kaolin sample [11]

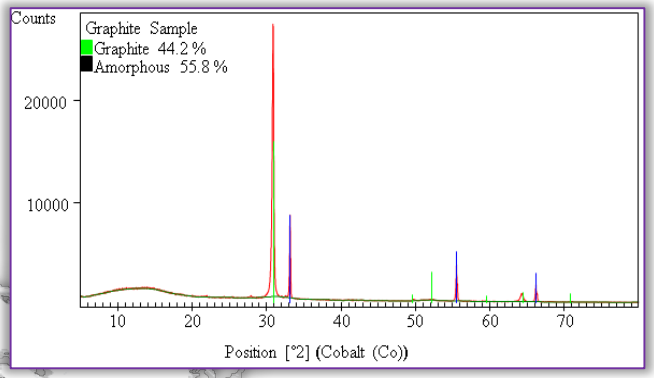

Figure 2. X-Ray Diffractometry Pattern (Phase Analysis) of graphite sample [11].

Table 1. XRD Results of kaolin and graphite sample showing the quantity of different phases present [11]

Materials	Kaolinite (wt. %)	Quartz (wt. %)	Amorphous wt. (%)	Graphite (wt. %)
Kaolin Sample	63.23	0.65	36.13	-
Graphite Sample	-	-	56.9	43.1

EXPERIMENTAL PROCEDURE

» **Composition calculation using the Rule of Mixtures Technique**

Rule of Mixtures is a method of approach to approximate estimation of composite material properties, based on an assumption that a composite property is the volume weighed average of the phases (matrix and dispersed phase). According to Rule of Mixtures [14] the density of composite materials are estimated as follows:

$$\rho_{mixture} = W_{tf\,kaolin} \times \rho_{kaolin} + W_{tf.graphite} \times \rho_{graphite} \quad (1)$$

$$M_{mixture} = \rho_{mixture} \times vol._{mould}. \quad (2)$$

where: $\rho_{mixture}$ represent density of the mixture, $M_{mixture}$ is the mass of the mixture, $W_{tf.\,kaolin}$ is the weight fraction of kaolin, ρ_{kaolin} is the density of kaolin, $W_{tf.graphite}$ is the weight fraction of graphite, $\rho_{graphite}$ is the density of graphite and $vol._{mould}$ is volume of mould.

» **Composites Production**

The raw materials in the samples making were 3:2vol. % of kaolin and graphite respectively with the addition of 2 and 4 (vol.) % titania respectively. The mixture were blended thoroughly for proper distribution of constituents materials in a ball mill for 3 hours at a speed of 72 rev/min after weighing via electronic weighing balance in accordance with the composition calculation initially prepared [11, 15]. The resulting blended compositions were mixed with 10% water of the amount of kaolin content in each composition, this was in order to enhance the plasticity of the mixture during compaction. The mixed samples were subjected to uniaxial compaction, which was carried out mechanically under pressure. The moulded materials were fired at varying temperatures (1300˚C, 1400˚C and 1500˚C). After which the samples were subjected to various test, to examine the phase analysis, evaluate their physical and mechanical properties.

» **Sintering Process**

The molded materials were fired at varying temperatures (1300°C, 1400°C and 1500°C) in an electric furnace. The rate of firing differs with increased temperature (room temperature to 500°C the sintering rate was 25°C/minute, 501°C to 1000°C the sintering rate was 10°C/minute while above 1000°C the sintering rate was 1°C/minute). On reaching the various sintering temperatures, the samples were held for one hour at the temperature before the furnace was switch off and the samples were allowed to cool in the furnace. The samples were subjected to various test to examine the phase analysis, evaluate their physical and mechanical properties.

Testing

» **Shrinkage Measurement**

The shrinkage properties of the pressed samples were determined by measuring both the green and fired dimensions, using a digital vernier caliper. The thickness and diameters were measured for evaluation and computation of the shrinkage [15].

$$\% \text{ linear shrinkage} = \frac{(Lg-Lf)}{(Lg)} \times 100 \quad (3)$$

where: Lg represent the green length and Lf represent the fired length.

$$\% \text{ volumetric shrinkage} = \frac{(Vg-Vf)}{(Vg)} \times 100 \quad (4)$$

where: Vg represent the green volume and Vf represent the fired Volume

» **Apparent porosity (AP)**

Test samples from each of the ceramic composite samples were dried out for 12 hours at 110˚C. The dry weight of each fired sample was taken and recorded as D. Each sample was immersed in water for 6 hours to soak and weighed while being suspended in air. The weight was recorded as W. Finally, the specimen was weighed when immersed in water [6, 15]. This was recorded as S. The apparent porosity was then calculated from the expression:

$$\% \text{ apparent porosity} = \frac{(W-D)}{(W-S)} \times 100 \quad (5)$$

» **Bulk Density**

The test specimens were dried out at 110˚C for 12 hours to ensure total water loss. Their dry weights were measured and recorded. They were allowed to cool and then immersed in a beaker of water. Bubbles were observed as the pores in the specimens were filled with water. Their soaked weights were measured and recorded. They were then suspended in a beaker one after the other using a sling and their respective suspended weights were measured and recorded [6, 15]. Bulk densities of the samples were calculated using the formula below:

$$\text{Bulk density} = \frac{D}{(W-S)} \quad (6)$$

where: D represent weight of dried specimen, S represent weight of dried specimen suspended in water, and W is weight of soaked specimen suspended in air.

» **Water Absorption**

The test sample was dried out in an oven till a constant weight of the sample was obtained. The sample was then placed in a vessel containing water in order to be completely submerged without touching the bottom of the vessel in which it is suspended. The vessel was then heated slowly so that the water boiled after heating. After boiling for about an hour with the evaporated water replaced, the sample was allowed to cool at room temperature for 24 hours. The sample was then renamed, blotted and then reweighed [15]. The percentage water absorption was calculated as showed below:

$$\% \text{ water absorption} = \frac{(\text{soaked wt} - \text{dried wt})}{(\text{dried wt})} \times 100 \quad (7)$$

» **Cold Compression Strength, Modulus of Elasticity and Absorbed Energy**

Cold compression strength test is to determine the compression strength to failure of each sample, an indication of its probable performance under load. The standard ceramic samples were dried in an oven at a temperature of 110˚C, allowed to cool. The cold compression strength tests were performed on INSTRON 1195 at a fixed crosshead speed of 10mm min^{-1}. Samples were prepared according to ASTM C133-97 (ASTM C133-97, 2003) [6, 15] cold crushing strength, modulus of elasticity and absorbed energy of standard and conditioned samples were calculated from the equation:

$$CCS = \frac{(\text{Load to fracture})}{(\text{Surface area of sample})} \quad (8)$$

RESULTS AND DISCUSSION

PHASE/MINERALOGICAL COMPOSITION OF THE RAW KAOLIN AND GRAPHITE SAMPLES

The phase/mineralogical composition of the kaolin and graphite samples were characterised (investigated)

with the aid of X-ray diffractometer. The results of the phase analysis of kaolin and graphite powder quantified by XRD were presented in Table 1, Figures 1 and 2. The phase/mineralogical composition of the raw materials used have been discussed extensively in [11] they are only reported for the purpose of showing that the compositions of the starting raw materials were known.

EFFECTS OF TITANIA (TiO_2) ADDITION

» Effects of Titania (TiO_2) Addition on the Phase Development in the Mullite-Carbon Ceramic Composite Samples Produced from Raw Kaolin and Graphite

The XRD results of the sintered samples are presented in Table 2 showing the various phases developed in the various sample at various sintering temperature.

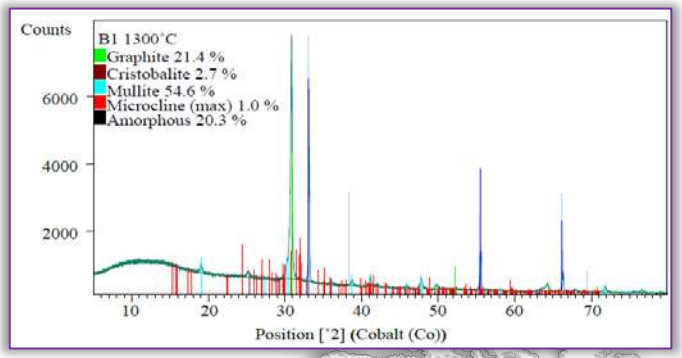

Figure 3. X-Ray Diffractometry Pattern of Sample B1 at 1300°C

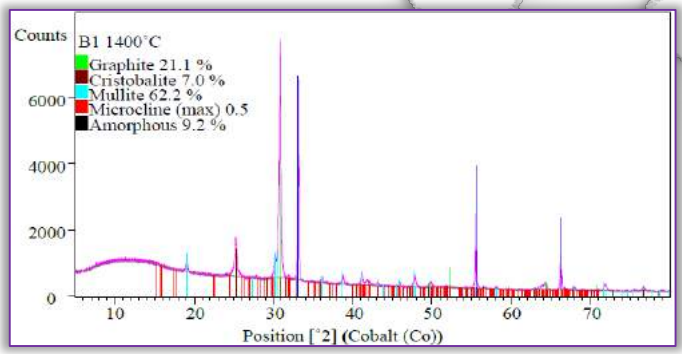

Figure 4. X-Ray Diffractometry Pattern of Sample B1 at 1400°C

Table 2. XRD Result of composition B1 and B2 sintered ceramic sample showing the quantity of different phases present.

Sample/ Sintering Temperature (°C)	Phase Developed (wt.%)				
	Graphite	Cristobalite	Mullite	Microcline	Amorphous
B1/1300	21.43	2.71	54.61	0.97	20.27
B1/1400	21.07	7.01	62.19	0.52	9.21
B1/1500	20.69	6.58	59.41	0.58	12.73
B2/1300	20.78	3.2	52.69	0.79	22.55
B2/1400	20.62	7.1	62.5	0.92	8.86
B2/1500	20.58	6.83	63.28	0.73	8.57

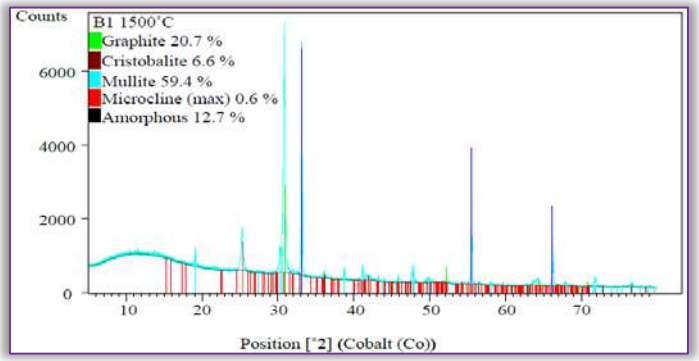

Figure 5. X-Ray Diffractometry Pattern of Sample B1 at 1500°C

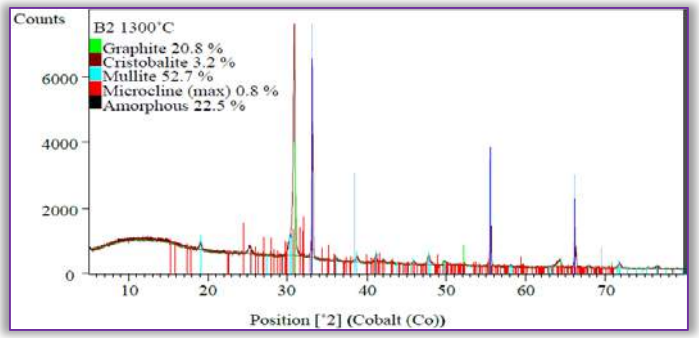

Figure 6. X-Ray Diffractometry Pattern of Sample B2 at 1300°C

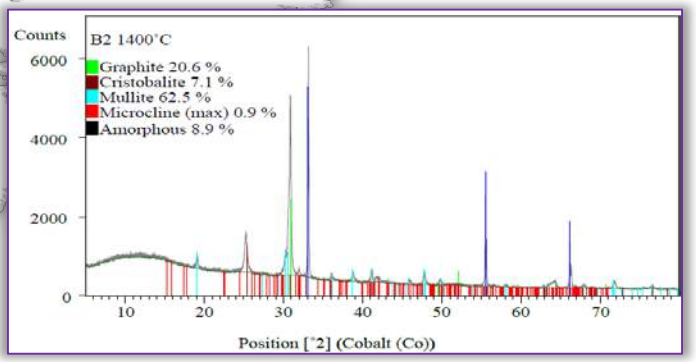

Figure 7. X-Ray Diffractometry Pattern of Sample B2 at 1400°C

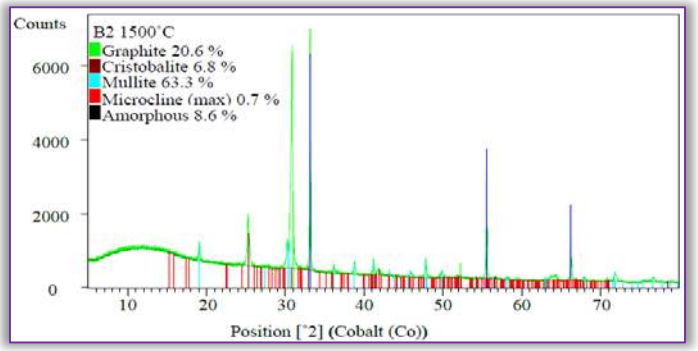

Figure 8. X-Ray Diffractometry Pattern of Sample B2 at 1500°C

Figure 3 to 5 which show the x-ray diffraction patterns of the samples with addition of 2% TiO_2, labelled as sample B1. While Figure 6 to 8 show the x-ray diffraction

patterns of the samples with addition of 4% TiO_2 to the raw kaolin and graphite, labelled as sample B2.

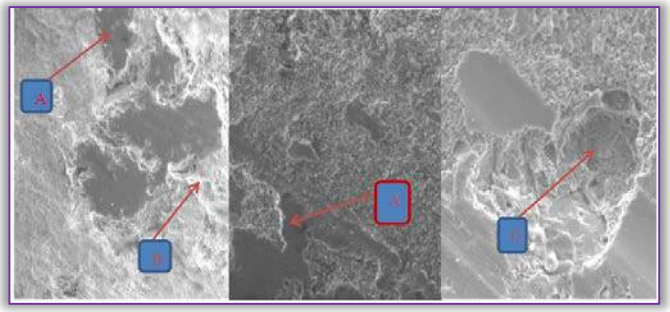

(a) (b) (c)

Plate 1. Typical SEM micrographs (Back Scattered Image) of Sample B1 showing its morphology at varied temperature (a) sample B1 at 1300˚C showing the Secondary Electron Image A = graphite phase and B = mullite phase, (b) sample B1 at 1400˚C showing the Secondary Electron Image of graphite phase and mullite phase (c) sample B1 at 1500˚C showing the Secondary Electron Image of graphite phase and C = mullite fibre Phase.

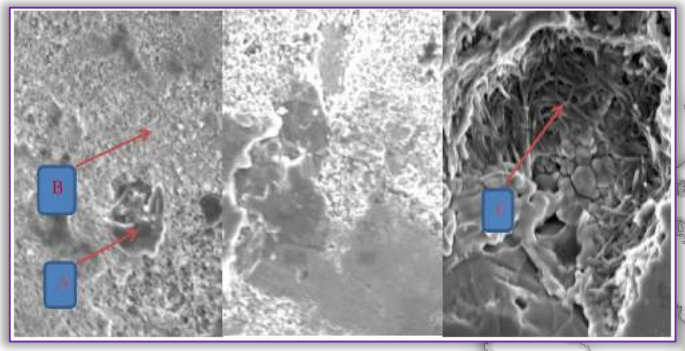

(a) (b) (c)

Plate 2. Typical SEM micrographs (Back Scattered Image) of Sample B2 showing its morphology at varied temperature (a) sample B2 at 1300˚C showing the Secondary Electron Image A= graphite phase and B= mullite phase, (b) sample B2 at 1400˚C showing the Secondary Electron Image of graphite phase and mullite phase (c) sample B2 at 1500˚C showing the Secondary Electron Image of graphite phase and C = mullite fibre Phase.

The XRD analysis, show that the sintered samples contains mullite, graphite, amorphous, cristobalite and microcline phases while plate 1 and 2 show the SEM morphology of the phase present in sample B1 and B2 respectively. With an increase in sintering temperature, the mullite phase of sample B1 increased rapidly from 1300˚C to 1400˚C and reduced slightly when the sintering temperature was raised to 1500˚C. Furthermore, cristobalite phase increased from 1300˚C to 1400˚C and reduced slightly when the sintering temperature was raised to 1500˚C.

This is due to mullitization process of the kaolinite contents of the kaolin which yields mullite and excess silica as the sintering temperature is increased beyond 900°C [6, 15, 16]. This expains the reasons why the mullite and cristobalite (a polymorph of silica) contents of the samples generally increased with increased sintering temperature Also, graphite reduced from 1300˚C to 1500˚C. Microcline reduced from 1300˚C to 1400˚C and increased slightly when the sintering temperature was raised to 1500˚C. Amorphous phase reduced from 1300˚C to 1400˚C and increased slightly when the sintering temperature was raised to 1500˚C. In sample B2, the mullite phase increased rapidly when the sintering temperature was raised from 1300˚C to 1500˚C. Also, cristobalite phase increased from 1300˚C to 1400˚C and reduced slightly when the sintering temperature was raised to 1500˚C.

The graphite reduced when the sintering temperature was raised from 1300˚C to 1500˚C. Microcline increased from 1300˚C to 1400˚C and reduced slightly below the amount attained at 1300˚C when the sintering temperature was raised to 1500˚C. Amorphous phase reduced from 1300˚C to 1500˚C. Moreover, many other researchers [17-21] have reported on the various transformations occur when kaolinite is fired from temperature just below 200°C to around 1000°C; this includes dehydration, dehydroxylation annd structural breakdown. As seen from Table 2, the raw Okpella kaolin's constituents are; 63.23% kaolinite, 0.65% quartz, 36.13% amorphous which undergo a series of high temperature phase transformation as the temperature was raised from 1300-1500˚C, the sintering reactions take place via;

$$Si_2Al_2O_5(OH)_4 \xrightarrow{\sim 420\text{-}660^{\circ}C} Al_2O_3{\cdot}2SiO_2 + 2H_2O$$

which involves the combination of two OH groups to form H_2O and oxygen which remains incorporated in metakaolin. At about 900˚C, metakaolinite decomposes to amorphous $SiO_2$and γ-Al_2O_3–type spinel via

$$Al_2O_3{\cdot}2SiO_2 \xrightarrow{900^{\circ}C} \gamma\text{-}Al_2O_3 + 2SiO_2$$

γAl_2O_3-type spinel and SiO_2 recrystallize into mullite at temperatures above 1100˚C via

$$3\gamma\text{-}Al_2O_3 + 2SiO_2 \xrightarrow{>1100^{\circ}C} 3Al_2O_3{\cdot}2SiO_2$$

Srikrishna, *et al*. (1990) [22], reported the formation of a single phase (with composition close to mullite) and excess SiO_2 at 900˚C. Thus the formation of mullite begins at temperatures >900˚C and the process continues till 1000˚C. Kausik *et al*. (2004) and Omani *et al*. (2000) [23, 24] reported that mullitization can be increased by catalytic ions such as Fe^{3+} and Ti^{4+}. These metallic ions help in mullite formation by replacing the Al^{3+} ions in the glass structure during firing. The presence of Ti^{4+} from the addition of TiO_2 modifies the chemical composition of the ceramic bodies and therefore the sintering behaviour is characterized by mullitization. The excess silica left during transformation of metakaolin to aluminium-silicon spinel at 925˚C-950˚C and also as a result of crystalline cristobalite formed along with platelet mullite during spinel transformation at 1050˚C.

» **The Effects of Titania (TiO_2) Addition on the Physical and Mechanical properties of Mullite-Carbon Ceramic Composite Samples Produced from Raw Kaolin and Graphite**

Evaluation of the effects of (2 and 4) vol. % titania addition on various physical and mechanical properties of ceramic composite samples sintered at varied sintering temperature. Below are the results of various physical and mechanical properties of samples (B1, B2).

≡ **Apparent Porosity**

The effect of sintering temperature on the apparent porosity (AP) of Samples (B1 and B2) with varied amount (2 and 4 vol. %) of TiO_2 addition is clearly shown in Figure 9 and Table 3. From the Figure, it is observed that the apparent porosity of sample B1 (2% titania) at various sintering temperature is higher than that of the sample B2 (4% titania). it is also observed that the apparent porosity of sample B1 at 1300˚C is 31.667%, as the sintering temperature increased to 1400˚C the AP slightly reduced to 30.743% further increase in the sintering temperature to 1500˚C leads to an increase in the apparent porosity of the sample to 31.49%. The apparent porosity of sample B2 when sintered at 1300˚C is 27.289%, as the sintering temperature increased to 1400˚C the AP slightly increased to 27.748% further increase in the sintering temperature to 1500˚C leads to an increase in the apparent porosity of the sample to 31.309%. It is observed that the AP level of sample B1 reduced from 1300˚C to 1400˚C further increase in the sintering temperature to 1500˚C leads to an increased in the AP. This implies that the densification of the sample continues from 1300˚C to 1500˚C but well pronounce at 1400˚C this indicate that the maximum densification is achieved at 1400˚C, an increase in the temperature from 1400˚C leads to reduction in densification of the sample. For sample B2, the AP keeps increasing when the sintering temperature was raised from 1300˚C to 1500˚C. This implies that the densification of the sample reduces from 1300˚C to 1500˚C.

Generally, the densification of B2 samples is better at all temperature than B1 samples. It is observed that the apparent porosity of sample B2 is better than sample A, while sample A is better than sample B1 at all temperatures. This implies that 4 vol. % titania aids densification of the sample, with less pores. According to Calister, (2007) [25] voids exist between particles of the newly formed green (unfired) ceramic, much of these inter-particles voids are eliminated during firing/sintering to produce sintered ceramic. Furthermore, according to some other researchers [16, 17, 26], the decrease in the value of AP from 1300˚C to 1400˚C is because of additional increase in the filling of spaces between bigger particles contained in the ceramic samples. The drastic increase in the apparent porosity from 1400˚C to 1500˚C is as a result of carbon reaction with oxygen, the carbon burnt off, leaving pores within the samples. According to Sadrnezhaad *et al*. (2006 and 2007) [27, 28] and Nemati *et al*. (2005) [29], high temperature oxidations of graphite lead to drastic deterioration due to graphite diminution, which result to pores in the samples.

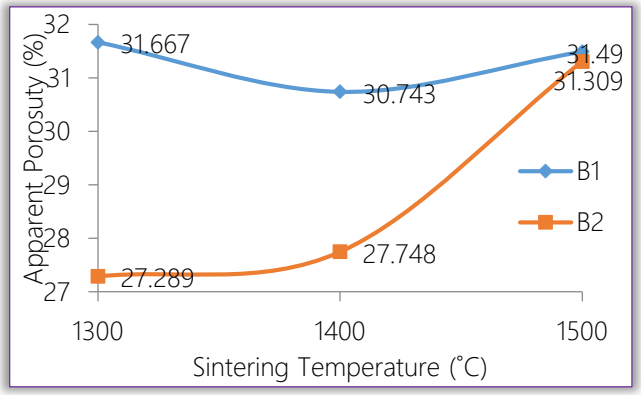

Figure 9. Effects of Sintering Temperature on Apparent Porosity of Sample with varied addition of TiO_2.

≡ **Bulk Density**

The effect of sintering temperature on the bulk density of the samples (B1 and B2) with varied amount (2 and 4 vol.%) of TiO_2 addition is clearly shown in Figure 10 and Table 3. From the Figure, it is observed that the bulk density of sample B1 at 1300˚C is 1.59gcm^{-3} as the sintering temperature increased to 1400˚C the bulk density slightly increased to 1.667gcm^{-3} further increase in sintering temperature to 1500˚C, the bulk density slightly reduced to 1.665gcm^{-3}. Also, the bulk density of sample B2 at 1300˚C is 1.891gcm^{-3} as the sintering temperature increased to 1400˚C the bulk density slightly reduced to 1.796gcm^{-3} further increase in sintering temperature to 1500˚C, the bulk density slightly reduced to 1.639gcm^{-3}. The bulk density of sample B1 and B2 are dictated by their apparent porosity, the sample with less pore is more dense. Generally, it can be deduce that the bulk density of B2 samples are higher than B1 samples due to their low porosity, this implies that the addition of 4 vol. % titania aids densification of the sample than 2 vol. % titania. According to Chandra *et al.* (2013) [7], substantial increase in bulk density was achieved with titania addition in the compacted sintered samples, which could be related to the influence of relatively higher density of TiO_2 itself. Furthermore, according to Aramide, (2012) and Brasileiro *et al.* (2006) [17, 26], the increase in bulk density is because of additional increase in the filling of spaces between bigger particles contained in the ceramic samples.

Summarily, samples with 4 vol. % titania (B2) attained maximum densification at 1300°C while the samples with 2 vol. % titania (B1) attained maximum densification at 1400°C.

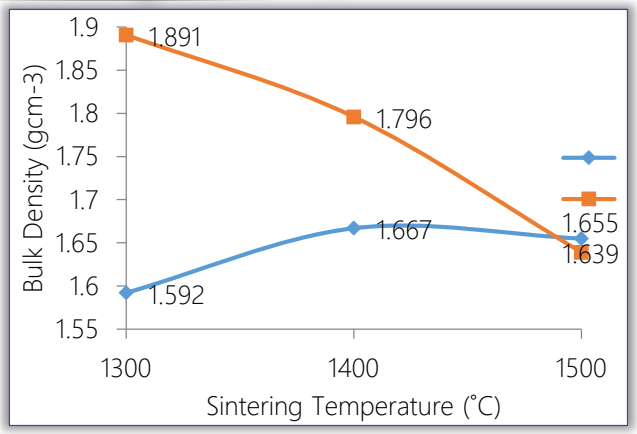

Figure 10. Effects of Sintering Temperature on the Bulk Density of Samples with varied TiO_2 addition.

≡ Water Absorption

The effect of sintering temperature on water absorption of the samples (B1 and B2) with varied amount (2 and 4 vol. %) of TiO_2 addition is clearly shown in Figure 11.

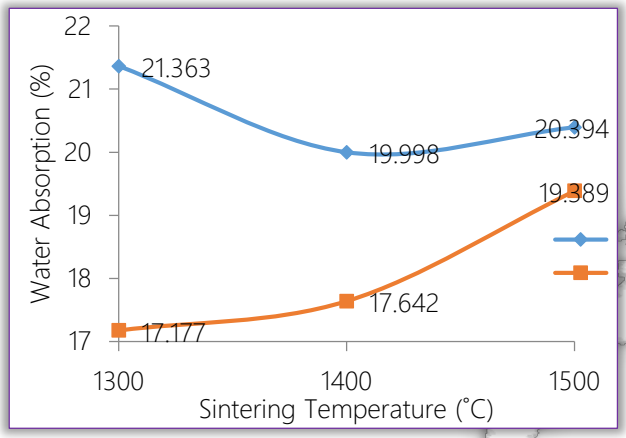

Figure 11. Effects of Sintering Temperature on the Water Absorption of Samples with varied TiO_2 addition.

From the Figure, it is observed that the water absorption of the sintered ceramic sample B1 is 21.363% at 1300˚C, with an increase in temperature to 1400˚C, the water absorption reduced to 19.998%. However, further increase in sintering temperature to 1500˚C, the water absorption of the sample increased to 20.394%. This followed the trend recorded for apparent porosity, which implies that the water absorption of the sample reduced when the sintering temperature was increased from 1300˚C to 1400˚C and later increased when the sintering temperature was raised to 1500˚C. For sintered ceramic sample B2, the water absorption is 17.177% at 1300˚C, with an increase in temperature to 1400˚C, the water absorption increased to 17.642%. However, further increase in sintering temperature to 1500˚C, the water absorption increased to 19.389%. This is because high temperature transformation of mullite and cristobalite in addition to some amount of carbon burn off leads to increased porosity as a result of reduced matter content of the samples. This is due to the sintering process; according to Calister, (2007) [25] voids exist between particles of the newly formed green (unfired) ceramic, much of these inter-particles voids are eliminated during firing/sintering to produce sintered ceramic. It is observed that the water absorption of sample B1 is higher at all temperature than B2.

≡ Cold Crushing Strength

The effect of sintering temperature on the cold crushing strength of samples (B1 and B2) with varied amount (2 and 4 vol.%) of TiO_2 addition is clearly shown in Figure 12 and Table 3. From the Figure, it is observed that the CCS of sample B1 at 1300˚C is 6.76Mpa, 7.99Mpa at 1400˚C and 7.65Mpa at 1500˚C. This implies that with an increase in the sintering temperature, the cold crushing strength significantly increased from 1300˚C to 1400˚C, further increase in the sintering temperature to 1500˚C leads to reduction in the CCS of the sample. Also, the CCS of sample B2 at 1300˚C is 8.68Mpa, 8.47Mpa at 1400˚C and 7.1Mpa at 1500˚C. This implies that with an increase in the sintering temperature, the cold crushing strength significantly reduced from 1300˚C to 1500˚C. This showed that the highest CCS of sample B1 is achieved at 1400˚C and B2 is achieved at 1300˚C. Generally, the cold crushing strength of sample B2 is better compared to sample B1 at 1300˚C and 1400˚C, with sample B1 only better at 1500˚C. The CCS results correspond to bulk density dictation which was affected by the porosity level of the sample. The reason for this is that an increase in bulk density of the sample, means that the sample contains more matter to bear the applied load [17, 18]. According to Brasileiro *et al.* (2006) [26], increase in CCS may be assigned to better filling of pores, higher bulk density and the increase amount of mullite that leads to improved mechanical properties.

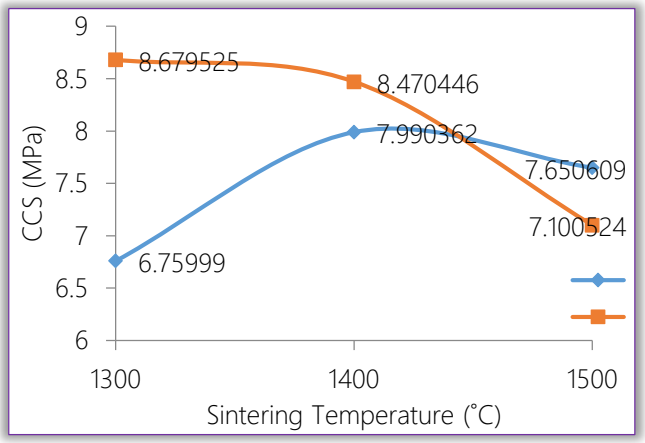

Figure 12. Effects of Sintering Temperature on the Cold Crushing Strength of Samples with varied addition of TiO_2.

≡ Modulus of Elasticity

The effect of sintering temperature on the modulus of elasticity (MOE) of samples (B1 and B2) with varied amount of TiO_2 addition is clearly shown in Figure 13 and Table 3. From the Figure, it is observed that the elastic modulus of sample B1 at 1300˚C is 60.431Mpa,

85.074Mpa at 1400˚C and 82.973Mpa at 1500˚C. This implies that with an increase in sintering temperature, the modulus of elasticity significantly increased from 1300˚C to1400˚C, further increase in the sintering temperature to 1500˚C, the MOE slightly reduced. Also, the modulus of elasticity of sample B2 at 1300˚C is 88.884Mpa, 88.584Mpa at 1400˚C and 68.033Mpa at 1500˚C. This implies that with an increase in sintering temperature, the modulus of elasticity slightly reduced from 1300˚C to 1400˚C, further increase in sintering temperature to 1500˚C, the MOE significantly reduced. Generally, the MOE of sample B2 is better compared to sample B1 at all temperatures. The MOE of the samples has the same trend with the CCS as dictated by the bulk density which was affected by the porosity level of the sample discussed earlier.

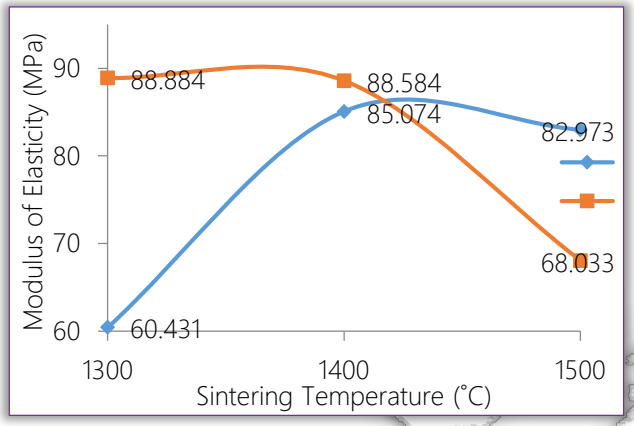

Figure 13. Effects of Sintering Temperature on the Modulus of Elasticity of Samples with varied addion of TiO_2.

≡ Absorbed Energy

The effect of sintering temperature on the absorbed energy (AE) of samples (B1 and B2) with varied amount of TiO_2 addition is clearly shown in Figure 13 and Table 3. From the Figure, it is observed that the absorbed energy of sample B1 at 1300˚C is 4.782J, 5.537J at 1400˚C and 5.488J at 1500˚C. This implies that with an increase in sintering temperature, the absorbed energy significantly increased from 1300˚C to 1400˚C, further increase in the sintering temperature to 1500˚C, the absorbed energy slightly reduced. Also, the absorbed energy of sample B2 at 1300˚C is 6.4926J, 6.063J at 1400˚C and 4.785J at 1500˚C. This implies that with an increase in sintering temperature, the absorbed energy slightly reduced from 1300˚C to 1400˚C, further increase in the sintering temperature to 1500˚C, the absorbed energy significantly reduced. The modulus of elasticity results shows that except from sample B1 at 1500˚C, sample B2 has higher MOE than B1 at 1300˚C and 1400˚C. The observed variation of absorbed energy with increased sintering temperature follows the same trend with that observed for the cold crushing strength as earlier discussed.

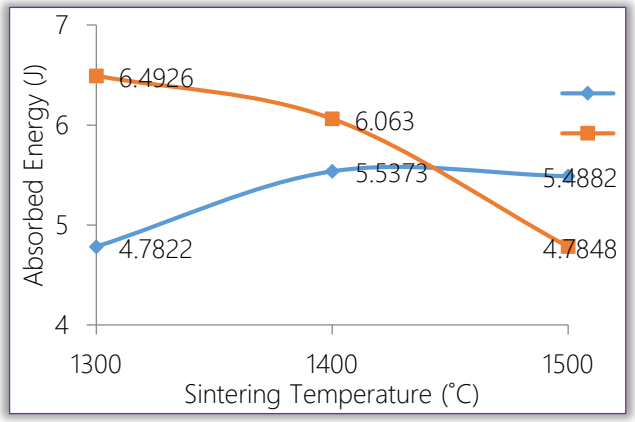

Figure 13. Effects of Sintering Temperature on the Absorbed Energy of Samples with varied addition of TiO_2.

≡ Linear Expansion

The effect of sintering temperature on the linear expansion of samples (B1 and B2) with varied amount of TiO2 addition is clearly shown in Figure 14 and Table 3. From the Figure, it is observed that the linear expansion of sample B1 is 1.018% at 1300˚C, 0.442% at 1400˚C and 2.216% at 1500˚C.

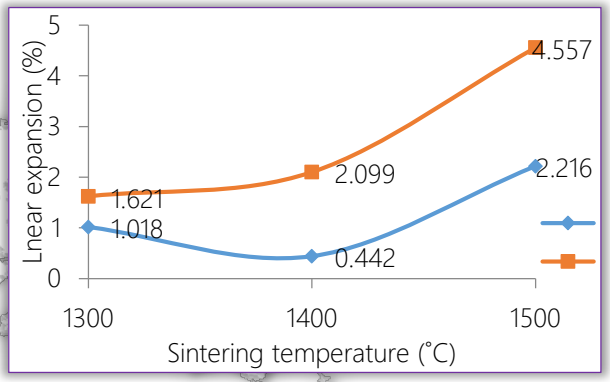

Figure 14. Effects of Sintering Temperature on the Linear Expansion of Samples with varied addition of TiO_2.

The linear expansion of sample B1 reduced significantly as sintering temperature increases from 1300˚C to 1400˚C, further increase in the sintering temperature to 1500˚C, the linear expansion of the sample significantly increased. Also, the linear expansion of sample B2 significantly increased when the sintering temperature was raised from 1300˚C to 1500˚C. Apart from sample B1 that reduced from 1300 to 1400, increase in sintering temperature leads to an increase in the linear expansion of the samples. Sample B1 has lower linear expansion than B2 samples at all temperature. The shrinkage due to cristobalite and mullite transformation was first compensated for by the graphite expansion before the sample later expand. Graphite has $0.6\text{-}4.3\times10^{-6}m/mk^{-1}$ as coefficient of linear expansion, the expansion was clearly recorded as an increment in the length of the samples after sintering. According to Grim, (1971) [30] during sintering process, the porosity of the ceramic body is reduced due to the vacancies and pores filling by molten (glassy phase). So, shrinkage size is equal to size

of pore removed or lost. Sintering temperature has an extreme effect on the value of linear shrinkage as increasing sintering temperature leads to increases linear shrinkage due to increasing amount of molten filling pores and product high shrinkage in the sample. The limited expansion recorded makes the composite (B1 and B2) suitable for high temperature applications.

≡ **Volumetric Shrinkage**

The effect of sintering temperature on the volumetric shrinkage of samples (B1 and B2) with varied amount of TiO_2 addition is clearly shown in Figure 15 and Table 3. From the Figure, it is observed that the volumetric shrinkage of sample B1 is 4.325% at 1300˚C,5.295% at 1400˚C and 5.673% at 1500˚C.

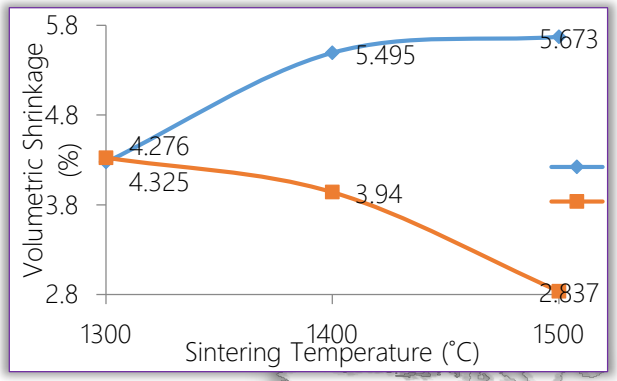

Figure 15. Effects of Sintering Temperature on Volumetric Shrinkage of Samples with varied addition of TiO_2.

Table 3. Mechanical Properties of the Sintered Ceramic Samples

Temp. (˚C)	Cold crushing strength (Mpa)	Modulus of elasticity (Mpa)	Absorbed energy (%)	Apparent porosity (%)	Bulk density (g/cm3)	Linear expansion (%)	Volumetric shrinkage (%)
B1/ 1300	6.75999	60.431	4.7822	31.667	1.592	1.018	4.276
B1/ 1400	7.99036	85.074	5.5373	30.743	1.667	0.442	5.495
B1/ 1500	7.65061	82.973	5.4882	31.490	1.655	2.216	5.673
B2/ 1300	8.67953	88.884	6.4926	27.289	1.891	1.621	4.325
B2/ 1400	8.47045	88.584	6.0630	27.748	1.796	2.099	3.940
B2/ 1500	7.10052	68.033	4.7848	31.309	1.639	4.557	2.837

With an increase in sintering temperature, the volumetric shrinkage of sample B1 significantly increased from 1300˚C to 1500˚C. Also, the volumetric shrinkage of sample B2 is 4.276% at 1300˚C, 3.94% at 1400˚C and 2.837% at 1500˚C. With an increase in sintering temperature, the volumetric shrinkage of sample significantly reduced from 1300˚C to 1500˚C. This implies that an increase in sintering temperature aids the volumetric shrinkage of sample B1 while volumetric shrinkage of sample B2 reduced when the temperature was raised from 1300˚C to 1500˚C. It is observed that the volumetric shrinkage of sample B2 is lower than B1 at all temperatures. This is because the carbon content of sample B1 is higher than sample B2.The limited shrinkage recorded makes the composite suitable for high temperature applications. According to Gupta, (2010) [31], a refractory material should be able to maintain sufficient dimensional stability at high temperatures and after/during repeated thermal cycling.

CONCLUSIONS

From the discusses data it is concluded that;

- mullite and cristobalite (a polymorph of silica) contents of the samples generally increased with increased sintering temperature;
- addition of titania improves on the densification of the samples at various sintering temperatures;
- the addition of 4 vol. % titania to the sample aids densification at relatively lower sintering temperature than when 2 vol. % titania is added;
- the addition of 4 vol. % titania to the sample improves on the cold crushing strength of the samples sintered at relatively lower sintering temperature than when 2 vol. % titania is added;
- 2 vol. % titania in the sample leads to progressive increased volumetric shrinkage as the sintering temperature increased while, 4 vol. % titania leads to reduction in the volumetric shrinkage with increased sintering temperature;
- the optimum mechanical property of the ceramic samples produced was achieved with sample that contain 4 (vol.) % titania and sintered at 1300˚C.

Acknowledgments

The authors acknowledge the Science Initiative Group (SIG), based at the Institute for Advanced Study in Princeton, for the support of this research work through the Competitive Fund for Rise Graduates Phase I (Round 1 and 3). Without this fund, it would have been extremely difficult to achieve the objectives of this research work.

References

[1] Cannillo, V., Leonelli, C., Montorsi, M., Romagnoli, M. and Veronesi, P. 2003. Experimental Results and Numerical Modelling of the Fracture Behaviour of Ceramic Refractory Plates, Tile & Brick Int. 5 324-327.

[2] Temoche, F., Garrido, L.B. and Aglietti, E.F. 2005. Processing of Mullite–Zirconia Grains for Slip Cast Ceramics, Ceram. Int., 31, 917–22. 134
[3] Rendtorff, N. M., Garrido, L.B., Aglietti, E. F. 2008. Thermal shock behavior of dense mullite–zirconia composites obtained by two processing routes, Ceram. Int. 34(8), 2017-2024.
[4] Badiee, H., Ebadzadeh, T., and Golestani-Fard F., 2001. The Effect of Additives on Mullitization of Iranian Andalusite, 44th International Colloquium on Refractories, Achen, 126–130
[5] Ebadzadeh, T., Ghasemi, E. 2002. Effect of TiO_2 addition on the stability of t-ZrO_2 in mullite-ZrO_2 composites prepared from various starting materials, Ceramics International, 28(4) 447-450
[6] Aramide F.O., Alaneme K.K., Olubambi P.A., Borode J.O., 2014. Effects of 0.2Y-9.8ZrO_2 Addition on the Mechanical Properties and Phase Development of Sintered Ceramic produced from Ipetumodu Clay, ANNALS of Faculty Engineering Hunedoara – International Journal of Engineering, Vol 7, Issue 4, 343-352.
[7] Chandra, D., Das, G. C., Sengupta, U. and Maitra, S. 2013. Studies on the reaction sintered zirconia-mullite-alumina composites with titania as additive Cerâmica, 59, 487-494.
[8] Aksel, C. and Komicezny, F. 2001. Mechanical Properties and Thermal Shock Behaviour of PSR333 Alumina–Mullite–Zirconia Refractory Materials, Glass Int., 1, 16-18.
[9] Jiang Lan, Chen Xiao-yan, Han Guo-ming, Meng Yu, 2011. Effect of additives on properties of aluminiumtitanate ceramics, Trans. Nonferous Met. Soc. China, 21, 1574-1579
[10] Dong Xiu-zhen, Wang Yi-ming, Li Yue. 2008. Additives' effect on aluminium titanate ceramics J. China Ceramics, 44(1), 7–10.
[11] Aramide F.O., Akintunde I.B., Oyetunji A., (2016). Insitu Synthesis and Characterization of Mullite-Carbon Refractory Ceramic Composite from Okpella Kaolin and Graphite, Usak University Journal of Material Science, 25-42.
[12] Nabil, R. B. and Barbara, Z. 2012. Sample Preparation for Atomic Spectrometric Analysis: An overview. Advances in Applied science research, 3(3), 1733-1737
[13] Young R.A, Sakthivel A., Moss T.S., Paiva-Santos C.O., Rietveld analysis of X-ray and neutron powder diffraction patterns, School of physics, Georgia institute of technology, Atlanta, U.S.A. 1994.
[14] Surappa M.K. (2003): „Aluminium Matrix Composites: Challenges and Opportunities; Sadhana, 28, Parts 1 & 2; Pp. 319-334.
[15] Aramide, F. O. 2015. Effects of sintering temperature on the phase developments and mechanical properties ifon clay, Leonardo Journal of Sciences Issue 26, 67-82.
[16] Aramide F.O., Alaneme K.K., Olubambi P.A., Borode J.O., 2014. High Temperature Synthesis of Zircon-Mullite-Zirconia Refractory Ceramic Composite from Clay Based Materials in Volume 5 - Composite, Ceramic, Quasi-crystals, Nanomaterials & Coatings: 2014--Sustainable Industrial Processing Summit & Exhibition/Shechtman International Symposium, held from 29 June - 04 July 2014, Fiesta Americana Condesa Cancun All Inclusive Resort, Cancun, Mexico, 155-176
[17] Aramide, F.O. 2012. Production and Characterization of Porous Insulating Fired Bricks from Ifon Clay with Varied Sawdust Admixture, Journal of Minerals and Materials Characterization and Engineering, 11, 970-975.
[18] Aramide, F.O. and Seidu, S.O. 2013. Production of Refractory Lining for Diesel Fired Rotary Furnace, from Locally Sourced Kaolin and Potter‟s Clay, Journal of Minerals and Materials Characterization and Engineering, 1, 75-79.
[19] Qiu, G., Jiang, T., Li, G., Fan, X. and Huang, Z. 2004. Activation and removal of silicon in Kaolinite by Thermo-chemical process, Scan. J. Metallurgy, 33, Pp.121-128.
[20] Gualtieri A.F. 2007. Thermal behavior of the raw materials forming porcelain stoneware mixtures by combined optical and in situ x-ray dilatometry J. Am Ceram Soc., 90, 1222-1231.
[21] McConville, C.J., Lee, W.E. 2005. Microstructural development on firing illite and smectite clays compared with that in kaolinite J. Am Ceram Soc., 88, 2267-2276.
[22] Srikrishna, K; Thomas, G; Martinez, R; Corral, M.P; Aza, S.D. and Moya, J.S. 1990. Kaolinite-Mullite reaction series: A TEM study, J. Mater., Sci., 25, 607-612.
[23] Kausik, D., Sukhen, D. and Swapan, K. D. 2004. Effect of substitution of fly ash for quartz in Triaxial kaolin-quartz–feldspar system, J. Eur. Ceram. Soc. 24, 3169-3175.
[24] Omani, H., Hamidouche, M., Madjoubi, M.A., Louci, K., Bouaouadja, N. and Etude, de-la. 2000. Transformation de trois nuances de kaolin en fonction de la temperature, Silicate Industriel, 65 (11–12), 119-124.
[25] Callister, W.D. 2007. Materials science and engineering: an introduction, 7th ed. John Wiley & Sons, Inc, 447.
[26] Brasileiro, M.I., Oliveira, D.H.S., Lira, H.L., Santana, L.N.L., Neves, G. A., Novaes, A.P., Sasak, J.M. 2006. Mullite Preparation from Kaolin Residue. Material Science Forum, 530-531, 625-630, 121.
[27] Sadrnezhaad, S.K., Nemati, Z.A., Mahshid, S., Hosseini S. and Hashemi, B. 2007. Effect of Al Antioxidant on the Rate of Oxidation of Carbon in MgO–C Refractory, Journal of the American Ceramic Society, 90(2), 509-515.
[28] Sadrnezhaad, S.K., Mahshid, S. Hashemi, B. and Nemati, Z.A. 2006. Oxidation Mechanism of C in MgO–C Refractory Bricks, Journal of the American Ceramic Society, 89(4), 1308-1316.
[29] Nemati, Z., Sadrnezhaad, S., and Mooghari, H.R.A. 2005. Effect of Ferrosilicon, Silicon and Aluminum Antioxidants on Microstructure and Mechanical Properties of Magnesia–Graphite Refractory, Refractories Applications & News, 10(6), 17-23.
[30] Grim Shaw R. W. 1971. "The chemistry and physics of clays and allied ceramic materials" Fourth edition. London.
[31] Gupta, O.P., 2010. Element of Fuels, Furnaces and Refractories, Romesh Chander Khanna Publishers 2-B, Nath market, NaiSarak Delhi India Fifth edition.